

Crystal structures and vibrational spectra of racemic and chiral 4-phenyl-1,3-oxazolidine-2-thione

Soh-ichi Kitoh,⁽¹⁾ Ko-Ki Kunimoto,^{(1)*} Norio Funaki,⁽¹⁾ Hitoshi Senda,⁽¹⁾
Akio Kuwae,⁽²⁾ and Kazuhiko Hanai⁽³⁾

Received October 31, 2001

The crystal structures of (*rac*)- and (*R*)-4-phenyl-1,3-oxazolidine-2-thione (4-POT) have been determined by X-ray diffraction. The structure of (*rac*)-4-POT is monoclinic $P2_1/n$ with $a = 11.9096(9)$ Å, $b = 5.9523(6)$ Å, $c = 12.3563(8)$ Å, $\beta = 91.054(6)^\circ$, $V = 875.8(1)$ Å³, and $Z = 4$. The structure of (*R*)-4-POT is orthorhombic $P2_12_12_1$ with $a = 7.7197(6)$ Å, $b = 21.603(2)$ Å, $c = 5.4613(9)$ Å, $V = 910.8(2)$ Å³, and $Z = 4$. (*rac*)-4-POT and (*R*)-4-POT crystals are shown to have different hydrogen-bonding patterns. In the racemic crystals, the enantiomeric (*R*)- and (*S*)-4-POT molecules are connected to form a cyclic dimer via the N—H...S hydrogen bond of the *cis* thioamide moiety [N...Sⁱ 3.438(2) Å, N—H...Sⁱ 176(2)°; symmetry code: (i) $1 - x, 1 - y, 1 - z$]. In the chiral (*R*)-4-POT crystals, the N—H...S intermolecular hydrogen bond forms a zigzag chain around the twofold screw axis [N...Sⁱⁱ 3.347(3) Å, N—H...Sⁱⁱ 161(3)°; symmetry code: (ii) $1/2 + x, 1/2 - y, 2 - z$]. Observed difference of 46°C in the melting points between the (*rac*)-4-POT and (*R*)-4-POT crystals is correlated with difference in the crystal packing. Vibrational spectra of (*rac*)- and (*R*)-4-POT crystals are discussed both in the solid state and in solution.

KEY WORDS: Crystal structure; 4-phenyl-1,3-oxazolidine-2-thione; vibrational spectra; crystal packing; intermolecular hydrogen bonds.

Introduction

Chiral auxiliary methodologies are proving to be increasingly useful for the asymmetric synthesis of many classes of compounds. Chiral 1,3-oxazolidine-2-ones and -2-thiones

have been developed as versatile and efficient auxiliaries.^{1,2} Recent studies have shown that usage of oxazolidine-2-thiones has some advantages as chiral auxiliaries compared to their 2-oxo analogues.³⁻⁵ Enantiomerically pure 1,3-oxazolidine-2-thiones are usually obtained through the reaction of chiral β -aminoalcohols and carbon disulfide.^{6,7} As an alternative route to chiral 2-thioxo-O,N-heterocycles, we have studied the optical resolution of racemic compounds through preferential crystallization. This methodology relies on the formation of conglomerate crystals, a separable mechanical mixture of the two pure enantiomers. Conglomerates

⁽¹⁾ Department of Chemistry and Chemical Engineering, Faculty of Technology, Kanazawa University, Kakuma-machi, Kanazawa 920-1192, Japan.

⁽²⁾ Institute of Natural Sciences, Nagoya City University, Mizuho-ku, Nagoya 467-8501, Japan.

⁽³⁾ Gifu Pharmaceutical University, Mitahora-higashi, Gifu 502-8585, Japan.

* To whom correspondence should be addressed. E-mail: lee@kenroku.kanazawa-u.ac.jp

usually show different physico-chemical behavior between racemates and racemic compounds owing to different intermolecular forces.

In search for the crystallization condition, we have found a difference of 46°C in the melting points between the (*rac*)- and the (*R*)-4-POT crystals. In the present study, the crystal structures of racemic and chiral 4-POT have been analyzed by X-ray crystallography in order to understand the intermolecular interactions in the two crystal systems. IR and Raman spectra of (*rac*)-4-POT and (*R*)-4-POT are measured and correlated with the molecular and crystal structures.

Experimental

Materials

(*R*)- and (*S*)-4-POT were prepared through the reaction of chiral phenylglycinol by using the published procedure.⁷ The reaction products were recrystallized from hot water several times. (*rac*)-4-POT was prepared by mixing equimolar (*R*)- and (*S*)-4-POT in acetone. The purities of these compounds were checked by the elemental analyses and ¹H NMR spectra. (*R*)-(-)- and (*S*)-(+)-phenylglycinol were purchased from Aldrich Chemical Co. Solvents and other chemicals were of reagent grade.

Spectroscopic measurements

The IR spectra were recorded on a Perkin-Elmer 1650 FT-IR spectrometer by averaging 64 scans with a resolution of 4 cm⁻¹. The spectra of solid samples were measured as KBr pellets and Nujol mulls. Either a 0.11-mm or a 1.0-mm path-length liquid cell with NaCl windows was used for solution samples.

The FT-Raman spectra were obtained on a Perkin-Elmer 2000R spectrometer equipped with a quartz beam splitter and InGaAs detector. The 1064-nm line of a Spectron Laser System SL300 Nd:YAG laser was used as the exciting source with an output power of about 200 mW at the

sample position. All spectra were accumulated for 60 scans with a resolution of 4 cm⁻¹.

Summary of physical and spectroscopic data

(*rac*)-4-POT. m.p.: 171.0–172.0°C; Anal. Calcd for C₉H₉NOS: C 60.31, H 5.06, N 7.81; Found: C 60.38, H 5.14, N 7.83; IR (KBr, cm⁻¹): 3191 (ν (N–H)), 1511 (ν (C–N) + δ (N–H)), 1178 (ν (C=S)); Raman (neat, cm⁻¹): 3171 (ν (N–H)), 1505 (ν (C–N) + δ (N–H)), 1168 (ν (C=S)); ¹H NMR (CDCl₃): δ 4.49 (dd, 1H, CH), 5.00 (t, 1H, CH₂), 5.12 (dd, 1H, CH₂), 7.36–7.46 (m, 5H, phenyl), 7.49 (s, 1H, NH).

(*R*)-4-POT. m.p.: 125.0–126.0°C; [α]_D²⁵: –32.00° (*c* 5.00, CHCl₃); Anal. Calcd for C₉H₉NOS: C 60.31, H 5.06, N 7.81; Found: C 60.27, H 5.09, N 7.78; IR (KBr, cm⁻¹): 3183 (ν (N–H)), 1522 (ν (C–N) + δ (N–H)), 1171 (ν (C=S)); Raman (neat, cm⁻¹): 3175 (ν (N–H)), 1531 (ν (C–N) + δ (N–H)), 1166 (ν (C=S)); ¹H NMR(CDCl₃): δ 4.49 (dd, 1H, CH), 5.00 (t, 1H, CH₂), 5.12 (dd, 1H, CH₂), 7.36–7.46 (m, 5H, phenyl), 7.49 (s, 1H, NH).

X-ray crystal structure analysis

(*rac*)- and (*R*)-4-POT crystals suitable for X-ray diffraction analysis were obtained by crystallization from aqueous acetone at room temperature. The absolute configuration of (*R*)-4-POT crystals was determined based on the absolute stereochemistry established previously.^{6,7} The preliminary cell dimensions and space group symmetry were determined photographically. X-ray diffraction data were obtained on a Rigaku AFC-5R diffractometer with a graphite monochromated Cu K α radiation ($\lambda = 1.54178 \text{ \AA}$). Intensity data were collected at room temperature (23 ± 1°C) with an ω –2 θ scan mode. An empirical absorption correction, based on azimuthal scans of several reflections, was applied which resulted in transmission factors ranging from 0.91 to 1.00 for (*rac*)-4-POT and from 0.76 to 1.00 for (*R*)-4-POT. The data were corrected for both Lorentz and polarization effects. Table 1 summarizes the crystal data

Table 1. Crystal Data and Structure Refinement

Compound	(<i>rac</i>)-4-POT	(<i>R</i>)-4-POT
CCDC deposit no.	CCDC-1003/6159	CCDC-1003/6160
Color/shape	Colorless/parallelepiped	Colorless/parallelepiped
Chemical formula	C ₉ H ₉ NOS	C ₉ H ₉ NOS
Formula weight	179.24	179.24
Temperature, K	296	296
Crystal system	Monoclinic	Orthorhombic
Space group	<i>P</i> 2 ₁ / <i>n</i>	<i>P</i> 2 ₁ 2 ₁ 2 ₁
Unit cell dimensions		
<i>a</i> (Å)	11.9096(9)	7.7197(6)
<i>b</i> (Å)	5.9523(6)	21.603(2)
<i>c</i> (Å)	12.3563(8)	5.4613(9)
β (deg)	91.054(6)	
Volume, Å ³	875.8(1)	910.8(2)
<i>Z</i>	4	4
Density(calculated), Mg/m ³	1.359	1.307
Absorption coefficient, mm ⁻¹	2.808	2.700
Diffractometer/scan	Rigaku AFC-5R/ω-2θ	Rigaku AFC-5R/ω-2θ
θ range for data collection, deg	3.57–59.92	4.09–59.99
Reflections measured	1530	850
Independent reflections	1453 (<i>R</i> _{int} = 0.025)	850
Observed reflections	1209 [<i>I</i> > 1.20σ(<i>I</i>)]	807 [<i>I</i> > 1.20σ(<i>I</i>)]
Data/restraints/parameters	1209/0/145	807/0/145
Goodness of fit	2.42	2.23
Final <i>R</i> indices [<i>I</i> > 1.20σ(<i>I</i>)]	<i>R</i> = 0.036, <i>wR</i> = 0.047	<i>R</i> = 0.034, <i>wR</i> = 0.042
Largest diff. peak and hole, e/Å ³	0.20, -0.32	0.13, -0.21

and experimental conditions for the crystal structure determination.

The structure was solved by direct methods using SIR88. Crystal structure analysis was performed by using the *teXsan* crystallographic software package.⁸ Non-hydrogen atoms were refined anisotropically. All the hydrogen-atom positions were found from a difference Fourier map and refined isotropically.

Results and discussion

Crystal structures of (*rac*)-4-POT and (*R*)-4-POT

The final positional and thermal parameters of (*rac*)-4-POT and (*R*)-4-POT for non-H atoms are presented in Table 2. Tables 3 and 4 summarize the bond lengths, bond angles, torsion angles, and the hydrogen-bonding geometries of the two crystals. As shown in Table 1, (*rac*)-4-POT and (*R*)-4-POT are crystallized in the

monoclinic and orthorhombic forms, respectively, with four molecules in a unit cell. Bond lengths and bond angles of (*rac*)-4-POT and (*R*)-4-POT are very similar to each other and comparable to that of nonsubstituted 1,3-oxazolidine-2-thione (OT).⁹ However, the thiocarbonyl C(1)–S(1) bond lengths are shorter than that of OT [1.656(2) and 1.652(3) Å for (*rac*)-4-POT and (*R*)-4-POT compared to 1.671(6) Å for OT]. As shown in Fig. 1, the oxazolidine ring conformations of the two crystals are slightly different from each other: the S(1)–C(1)–O(1)–C(3) fragment is almost planar with the C(2) atom on the opposite side of the ring. Thus the heterocyclic ring adopts the envelope conformation with the torsional angle S(1)–C(1)–N(1)–C(2) of -171.9(1)° for (*rac*)-4-POT and 172.8(2)° for (*R*)-4-POT.

The molecular packing in crystals is shown in Fig. 2. In both cases a short intermolecular contact between the H atom of one molecule and the S atom of a neighboring molecule is observed.

Table 2. Fractional Atomic Coordinates and Equivalent Isotropic Thermal Parameters

Atom	<i>x</i>	<i>y</i>	<i>z</i>	<i>B</i> _{eq} ^a (Å ²)
<i>(rac)</i> -4-POT				
S(1)	0.56633(4)	0.19455(9)	0.58045(4)	3.98(3)
O(1)	0.7690(1)	0.3336(2)	0.6294(1)	3.97(7)
N(1)	0.6661(1)	0.5942(3)	0.5536(1)	3.53(8)
C(1)	0.6676(2)	0.3852(3)	0.5866(1)	2.99(8)
C(2)	0.7756(2)	0.7032(4)	0.5585(2)	3.39(9)
C(3)	0.8391(2)	0.5333(4)	0.6292(2)	4.1(1)
C(4)	0.8247(1)	0.7372(3)	0.4482(2)	3.03(8)
C(5)	0.8802(2)	0.9341(4)	0.4238(2)	4.1(1)
C(6)	0.9295(2)	0.9621(5)	0.3244(2)	5.2(1)
C(7)	0.9232(2)	0.7966(5)	0.2481(2)	5.0(1)
C(8)	0.8667(2)	0.6017(5)	0.2706(2)	4.6(1)
C(9)	0.8180(2)	0.5718(4)	0.3697(2)	3.9(1)
<i>(R)</i> -4-POT				
S(1)	0.4034(1)	0.18887(3)	0.9843(2)	6.58(5)
O(1)	0.2708(3)	0.25589(9)	0.6327(5)	6.5(1)
N(1)	0.5023(3)	0.2969(1)	0.7901(5)	4.9(1)
C(1)	0.3959(4)	0.2494(1)	0.7999(6)	4.9(1)
C(2)	0.4692(4)	0.3382(1)	0.5846(6)	4.8(1)
C(3)	0.2862(5)	0.3161(2)	0.516(1)	6.5(2)
C(4)	0.4805(3)	0.4059(1)	0.6497(5)	3.9(1)
C(5)	0.5704(3)	0.4456(1)	0.4997(6)	4.6(1)
C(6)	0.5794(4)	0.5082(1)	0.5528(6)	5.2(1)
C(7)	0.5003(4)	0.5308(1)	0.7573(6)	5.1(1)
C(8)	0.4095(4)	0.4915(1)	0.9098(6)	5.1(1)
C(9)	0.4003(4)	0.4291(1)	0.8565(5)	4.6(1)

$$^a B_{\text{eq}} = (4/3) \sum_i \sum_j \beta_{ij} a_i \cdot a_j \cdot (a_i \cdot a_j).$$

However, the hydrogen-bonding pattern is quite different. In the crystal of *(rac)*-4-POT, the thioamide C=S group of an enantiomeric molecule is hydrogen-bonded to the thioamide NH group of a antipode molecule to form a centrosymmetric cyclic dimer [N(1)⋯S(1)ⁱ 3.438(2) Å, N(1)–H⋯S(1)ⁱ 176(2)^o; symmetry code: (i) 1 – *x*, 1 – *y*, 1 – *z*]. On the other hand, a zigzag chain is formed through the N–H⋯S intermolecular hydrogen bonding in the *(R)*-4-POT crystals [N(1)⋯S(1)ⁱⁱ

Table 3. Selected Bond Lengths (Å), Bond Angles (Deg), and Torsion Angles (Deg)^a

	<i>(rac)</i> -4-POT	<i>(R)</i> -4-POT
Bond length		
S(1)–C(1)	1.656(2)	1.652(3)
O(1)–C(1)	1.345(2)	1.337(4)
O(1)–C(3)	1.452(3)	1.452(4)
N(1)–C(1)	1.310(3)	1.315(4)
N(1)–C(2)	1.457(3)	1.456(4)
C(2)–C(3)	1.528(3)	1.537(5)
C(2)–C(4)	1.507(3)	1.508(4)
Bond angle		
C(1)–O(1)–C(3)	109.0(2)	109.5(2)
C(1)–N(1)–C(2)	113.8(2)	113.6(3)
S(1)–C(1)–O(1)	120.6(1)	121.6(2)
S(1)–C(1)–N(1)	129.1(2)	128.3(3)
O(1)–C(1)–N(1)	110.2(2)	110.0(3)
N(1)–C(2)–C(3)	99.3(2)	99.1(3)
N(1)–C(2)–C(4)	112.6(2)	113.7(2)
C(3)–C(2)–C(4)	114.2(2)	114.3(2)
O(1)–C(3)–C(2)	105.3(2)	104.3(3)
Torsion angle		
S(1)–C(1)–O(1)–C(3)	–177.3(1)	173.9(3)
S(1)–C(1)–N(1)–C(2)	–171.9(1)	172.8(2)
O(1)–C(3)–C(2)–N(1)	14.6(2)	–17.9(4)
O(1)–C(1)–N(1)–C(2)	7.6(2)	–7.4(3)
N(1)–C(2)–C(4)–C(5)	139.5(2)	134.2(3)
N(1)–C(2)–C(4)–C(9)	–42.0(3)	–46.6(3)
C(1)–O(1)–C(3)–C(2)	–11.8(2)	15.6(4)
N(1)–C(1)–O(1)–C(3)	3.2(2)	–5.9(4)
C(1)–N(1)–C(2)–C(3)	–14.0(2)	16.1(3)
C(3)–C(2)–C(4)–C(5)	–108.1(2)	–113.0(3)
C(3)–C(2)–C(4)–C(9)	70.3(2)	66.2(4)

^aEstimated standard deviations in the least significant figure are given in parentheses.

3.347(3) Å, N(1)–H⋯S(1)ⁱⁱ 161(3)^o; symmetry code: (ii) 1/2 + *x*, 1/2 – *y*, 2 – *z*]. In considering the D⋯A distance and the D–H⋯A angle, *(rac)*-4-POT crystals may have slightly more favorable hydrogen bonding than *(R)*-4-POT crystals. However, this small difference in the hydrogen-bonding strength cannot

Table 4. Hydrogen Bonding Geometry

Compound	D–H⋯A	D–H (Å)	H⋯A (Å)	D⋯A (Å)	D–H⋯A (deg)
<i>(rac)</i> -4-POT	N(1)–H⋯S(1) ⁱ	0.78(2)	2.66(2)	3.438(2)	176(2)
<i>(R)</i> -4-POT	N(1)–H⋯S(1) ⁱⁱ	0.86(4)	2.53(4)	3.347(3)	161(3)

Note: Symmetry codes: (i) 1 – *x*, 1 – *y*, 1 – *z*; (ii) 1/2 + *x*, 1/2 – *y*, 2 – *z*.

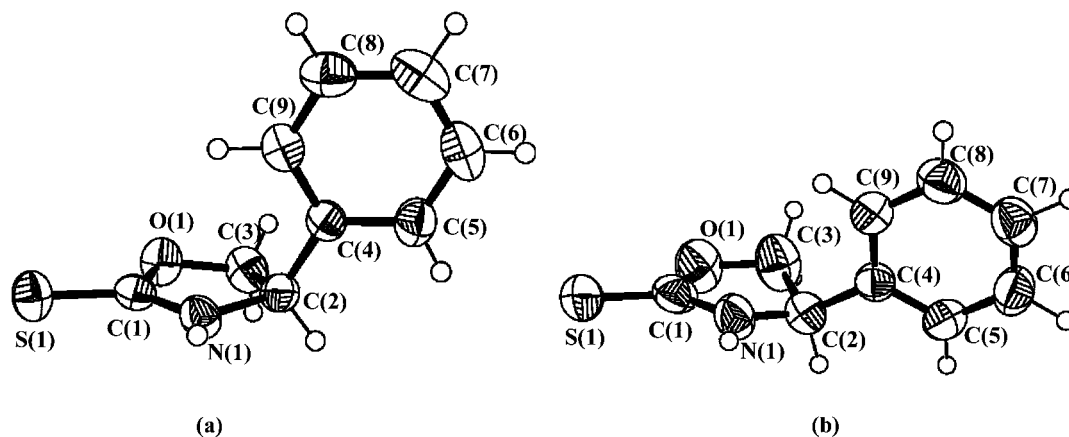


Fig. 1. ORTEP drawings of the (*R*)-4-POT molecules with the atom numbering: (a) in (*rac*)-4-POT crystals and (b) (*R*)-4-POT crystals. Thermal ellipsoids are drawn at the 50% probability level.

account for a large difference in the melting points (171.5°C for (*rac*)-4-POT and 125.5°C for (*R*)-4-POT). Closer crystal packing in (*rac*)-4-POT crystals is the main reason for the higher melting point for the crystals (calculated densities of (*rac*)-4-POT and (*R*)-4-POT are 1.359 and 1.307 Mg m⁻³, respectively).

IR and Raman spectra

IR spectrum of the nonsubstituted OT was first reported by Cristiani *et al.*¹⁰ They also carried out normal coordinate analyses of OT and its 2-one analogue to establish the band assignments.¹¹ Similar to OT, (*rac*)- and (*R*)-4-POT exhibit IR bands characteristic of the OT ring; the $\nu(\text{NH})$, the $\nu(\text{C}-\text{N}) + \delta(\text{N}-\text{H})$, and the $\nu(\text{C}=\text{S})$ bands are observed in the 3200, 1500, and 1170 cm⁻¹ regions, respectively. Assignment of the 1170 cm⁻¹ band to $\nu(\text{C}=\text{S})$ is tentative, because the calculation by Devillanova *et al.*¹¹ indicates that the C=S stretching mode in OT does not give the main contribution to the band at 1107 cm⁻¹, but to the band at 513 cm⁻¹. In the solid-state IR spectra, the $\nu(\text{NH})$ bands of hydrogen-bonded (*rac*)-4-POT and (*R*)-4-POT are observed at 3191 and 3183 cm⁻¹, respectively, close to that of OT. In the Raman spectra, these bands occur at 3171 and 3175 cm⁻¹, respectively. The $\nu(\text{N}-\text{H})$

difference between the free and the associated forms is often used as a measure of the hydrogen bonding strength. However, it is hard to correlate a frequency difference in the $\nu(\text{N}-\text{H})$ with the H-bonding strength, since (*rac*)-4-POT and (*R*)-4-POT have different intermolecular H-bonding patterns as shown in the X-ray result. The $\nu(\text{C}-\text{N}) + \delta(\text{N}-\text{H})$ and the $\nu(\text{C}=\text{S})$ bands are observed at 1511 and 1178 cm⁻¹ for (*rac*)-4-POT and at 1522 and 1171 cm⁻¹ for (*R*)-4-POT. In the Raman spectra, the corresponding bands are observed at 1505 and 1168 cm⁻¹ for (*rac*)-4-POT and at 1531 and 1166 cm⁻¹ for (*R*)-4-POT.

When dissolved in CHCl₃, the $\nu(\text{N}-\text{H})$ band of (*rac*)-4-POT is observed as a doublet at 3443 and 3189 cm⁻¹. On decreasing the concentration from 0.1 to 0.01 M stepwise, the intensity of the former gradually increases at the expense of the latter. Thus, the former and the latter bands are assigned to the $\nu(\text{N}-\text{H})$ of the free and the associated form, respectively. The band at 3189 cm⁻¹ undergoes a higher frequency shift to the 3209 cm⁻¹, while that of the free form remains unshifted. This concentration dependence of the $\nu(\text{N}-\text{H})$ of the associated form suggests that the chain-type hydrogen bonding occurs in CHCl₃ solution in contrast with the association in the crystal. In CHCl₃ solution, the $\nu(\text{C}-\text{N}) + \delta(\text{N}-\text{H})$ band around 1500 cm⁻¹ is also split into a doublet

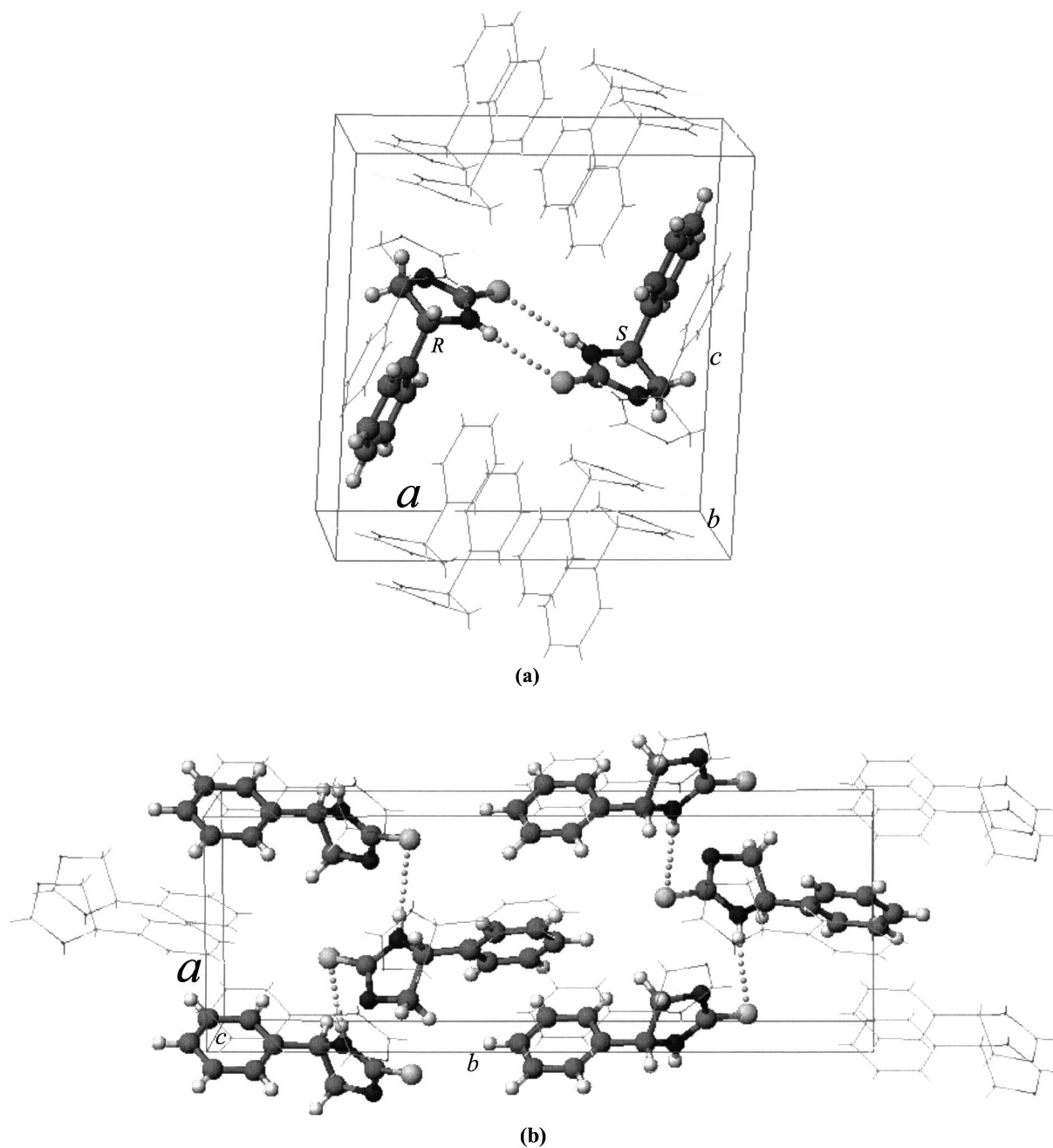


Fig. 2. Molecular packing (a) in (*rac*)-4-POT and (b) in (*R*)-4-POT crystals. The hydrogen bondings are indicated by dashed lines.

at 1519 cm^{-1} (shoulder) and at 1480 cm^{-1} (strong). Since the 1480 cm^{-1} band gains its intensity at the expense of the 1519 cm^{-1} band intensity, the higher frequency and the lower frequency

bands can be assigned to the $\nu(\text{C-N}) + \delta(\text{NH})$ mode of the associated and the free species, respectively. (*R*)-4-POT in CHCl_3 solution shows similar IR spectra; the spectral behavior implies

that the molecule also assumes the chain-type hydrogen bonding in concentrated solution.

References

1. Evans, D.A.; Weber, A.E. *J. Am. Chem. Soc.* **1986**, *108*, 6757.
2. Nagao, Y.; Yamada, S.; Kumagai, T.; Ochiai, M.; Fujita, E. *J. Chem. Soc., Chem. Commun.* **1985**, 1418.
3. Fujita, E.; Nagao, Y. *Adv. Heterocycl. Chem.* **1989**, *45*, 1, and references cited therein.
4. Crimmins, M.T.; King, B.W. *J. Am. Chem. Soc.* **1998**, *120*, 9084.
5. Masuda, R.; Hojo, M.; Ichi, T.; Sasano, S.; Kobayashi, T.; Kuroda, C. *Tetrahedron Lett.* **1991**, *32*, 1195.
6. Delaunay, D.; Toupet, L.; Le Corre, M. *J. Org. Chem.* **1995**, *60*, 6604.
7. Li, G.; Ohtani, T. *Heterocycles*, **1997**, *45*, 2471.
8. *teXsan, Crystal Structure Analysis Package*; Molecular Structure Corp.: The Woodlands, TX, 1985.
9. Li, L.; Zhong, H. *Jiegou Huaxue (J. Struct. Chem.)* **1986**, *5*, 52.
10. Cristiani, F.; Devillanova, F.A.; Verani, G. *J. Chem. Soc., Perkin II* **1977**, 324.
11. Devillanova, F.A.; Verani, G.; Gayathri Devi, K.R.; Sathyanarayana, D.N. *Spectrochim. Acta* **1980**, *36A*, 199.